Pergamon

Geochimica et Cosmochimica Acta, Vol. 66, No. 3, pp. 417–429, 2002

0016-7037/02 $22.00 + .00

PII S0016-7037(01)00792-X

A model of oscillatory zoning in solid solutions grown from aqueous solutions: Applications to the (Ba,Sr)SO_4 system

IVAN L'HEUREUX[1,*] and BJØRN JAMTVEIT[2]

[1]Department of Physics, 150 Louis Pasteur, University of Ottawa, Ottawa, ON K1N 6N5, Canada
[2]Department of Geology, University of Oslo, P.O. Box 1047 Blindern, N-0316 Oslo, Norway

(*Received November* 17, 2000; *accepted in revised form July* 20, 2001)

Abstract—Barite-celestite crystals can be synthesized from aqueous solutions during counter-diffusion in a gel column connecting two reservoirs. It is known that such crystals may exhibit oscillatory zoning, whereby the barium composition in the crystal fluctuates more or less regularly from the core of the crystal to its rim. We present here a simple model of oscillatory zoning in such binary solid solutions A_1A_2 grown from aqueous solutions. The model combines diffusive transport of the relevant ions with an autocatalytic growth process. The latter is formulated as a continuous growth in which the probability of finding a kink site on the growing surface depends on the chemical composition of that surface. Thus, an A_1-rich surface favors the growth of A_1 over A_2, as long as A_1 is present in the vicinity of the surface. Precipitation results in a local depletion of A_1 in the aqueous solution, and the system may switch to a A_2 growth mode, until diffusion replenishes the amount of A_1, and so on. We use a dynamical equation for the molar fraction of component A_1 in the crystal, which results from mass conservation across the rough crystal-solution interface. Linear stability analysis and direct numerical solutions show that the system exhibits oscillatory behavior. Using the barite-celestite system as a framework, the scaling is consistent with the experimental observations. We discuss the variety of zoning patterns and textures numerically obtained as the concentrations of reactants in the reservoirs vary. This model might help in understanding the formation of oscillatory zoning in hydrothermal environments. *Copyright © 2002 Elsevier Science Ltd*

1. INTRODUCTION

Many minerals exhibit intracrystalline oscillatory zoning, whereby their chemical compositions vary up and down along a crystal core-to-rim profile. Perhaps the best known example of a mineral commonly exhibiting oscillatory zoning is plagioclase feldspar, a solid solution series between the end-members anorthite and albite (see, e.g., Pearce et al., 1987; Pearce and Kolisnik, 1990). Here, the anorthite content varies on a scale of tens of microns along a core-to-rim profile perpendicular to a growing face. Oscillatory zoning may also manifest itself as variations of trace elements in a mineral, for example, Mn in calcite (Reeder et al., 1990). Traditionally, it was believed that oscillatory zoning is a relatively rare occurrence. However, with the development of more sophisticated observation techniques, it has been recently recognized (Shore and Fowler, 1996) that oscillatory zoning may occur in all major classes of minerals and in a wide range of geological environments (igneous, sedimentary, metamorphic, and water-rock systems).

Understanding the origin of such pattern formation is important, as it can provide information on the genesis of the mineral and the geological history of its host rock. For instance, it can be used to understand magmatic processes in silicate melts, or it can give us relevant information about the nature of fluid-rock interactions in hydrothermally grown minerals.

Oscillatory zoning may result from the response to systematic or random variations in the external parameters controlling the growth environment (Holten et al., 2000; Katsev and L'Heureux, 2000). However, other mechanisms are possible. It is known that spatio-temporal patterns can arise spontaneously without external templates, i.e., by self-organization (Cross and Hohenberg, 1993; Ortoleva 1994). In fact, modeling the kinetics of crystal growth naturally provides nonlinear coupling schemes between the various dynamic variables that are necessary to generate a self-organized pattern.

The first quantitative model of self-organized oscillatory zoning (for plagioclase) was proposed by Haase et al. (1980). Their model was based on an unspecified autocatalytic growth process in a diffusing silicate melt. Strictly periodic zoning could be obtained with their model. Later, Allègre et al. (1981) proposed a model of oscillatory zoning in plagioclase in which the growth kinetics are modified by a time delay introduced by the structural rearrangement in a diffusing silicate melt. They found an approximate solution exhibiting a (damped) oscillatory behavior, but no self-induced oscillations. In the contributions by Wang and Merino (1990, 1992, 1993, 1995), the diffusive transport equation is integrated over an unspecified boundary layer to generate a simpler ordinary differential equation. This procedure, coupled with appropriate growth rate expressions, was applied to various systems (agate, plagioclase, trace elements in calcite). Self-induced oscillations were generated in all cases for constrained but realistic parameter values. More recently, Wang and Wu (1995) proposed another oscillatory zoning model (for plagioclase) in which the solid phase concentration of each component is proportional to its growth velocity. An effective nonequilibrium partitioning coefficient between the concentration in the solid phase and the one in the adjacent melt was thus computed. Although only the infinite-diffusion and the no-diffusion cases were considered, self-organized oscillatory solutions were obtained. Another self-organized oscillatory zoning model was proposed by

* Author to whom correspondence should be addressed (ilheureu@physics.uottawa.ca).

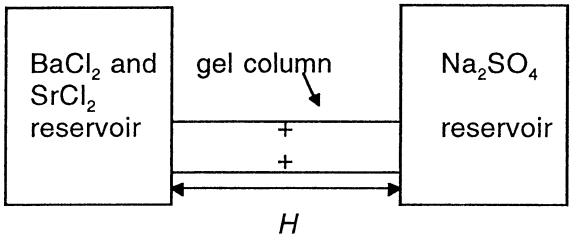

Fig. 1. Schematic representation of the experiments performed by Putnis et al. (1992) and Prieto et al. (1993, 1997). The experiment produced synthetic crystals of $(Ba,Sr)SO_4$ (symbolized by plus signs) in a gel column of length $H = 28$ cm connecting two reactant reservoirs.

Table 1. Observed zoning profiles from core to rim for various reservoir concentrations (from Prieto et al., 1993).

Initial reservoir concentrations (M) Na_2SO_4-$BaCl_2$-$SrCl_2$	Nature of profile
1) 0.5-0.5-0.5	Oscillatory zoning
2) 0.3-0.5-0.5	Oscillatory zoning
3) 0.5-0.3-0.3	Oscillatory zoning
4) 0.3-0.3-0.3	Ba rich to Sr rich to Ba rich
5) 0.1-0.5-0.5	Ba rich to Sr rich to Ba rich
6) 0.1-0.3-0.3	Ba rich to Sr rich to Ba rich
7) 0.1-0.3-0.1	Barite
8) 0.1-0.1-0.3	Ba rich to Sr rich to Ba rich, or Sr rich to Ba rich

L'Heureux (1993) and L'Heureux and Fowler (1996) in which the diffusion equation was solved in a silicate melt with realistic growth kinetics and a nonequilibrium partitioning coefficient (considered as a free parameter). There, self-organized oscillatory solutions were obtained. As the partitioning coefficient was varied, a period doubling sequence to a chaotic regime was obtained.

All these models are deterministic. However, analysis of natural data suggests that random fluctuations in the environment in which the crystal grows may play a significant role (Holten et al., 1997). In the case of nonequilibrium crystal growth, one clearly needs to consider both the internal growth dynamics and their sensitivity to external random fluctuations, and recent studies have focused on the sensitivity of nonlinear crystal growth processes to external noise (Holten et al., 2000; Katsev and L'Heureux, 2000). However, such studies clearly require detailed knowledge about the processes involved in nonequilibrium crystal growth of solid solutions. Such information is largely lacking for the most common rock-forming minerals.

Experimentally produced oscillatory mineral zonation has, however, been studied extensively for barite-celestite solid solution $(Ba,Sr)SO_4$ by Putnis et al. (1992), Prieto et al. (1993, 1997), and Pina et al. (2000). These researchers achieved growth of $(Ba,Sr)SO_4$ (for which the end-members' solubilities are very different) by counter-diffusion in aqueous solutions. Figure 1 illustrates a typical experimental setup. Two reservoirs containing $BaCl_2$ and $SrCl_2$ solutions on one hand and Na_2SO_4 solution on the other are connected by a gel column of length $H = 28$ cm. Through diffusional transport, the concentrations of the reactants increase in the gel column, resulting eventually in nucleation and growth of $(Ba,Sr)SO_4$ crystals. After 1 month of growth, the morphology of the resulting crystals was studied by scanning electron microscopy. Table 1 presents the various zoning textures reported by Prieto et al. (1993) with the corresponding reservoir concentrations. In the cases where the concentrations of the reservoir solutions are large, oscillatory zoning was observed. This zoning is characterized by local fluctuations of Ba composition over scales of 1 to 10 μm. These experiments have thus allowed the characterization of the growth process both in terms of the time scales involved and the supersaturation states during the growth process.

This system thus seems to be a natural starting point for developing a crystal growth model leading to oscillatory pattern formation in a binary solid solution A_1A_2 growing from aqueous solutions. Such a model may be tested against observations from experiments performed under controlled conditions. Our model is based on a continuous growth mechanism with a growth rate expression that includes terms related to the probability of finding a kink site for the growth of component A_1 ($BaSO_4$, for example) or A_2 ($SrSO_4$, for example) onto the crystal surface. In general, these probabilities depend on the local chemical composition of the surface. The proposed growth mechanism has the characteristics of an autocatalytic process. Thus, it is expected that an A_1-rich surface will favor the growth of A_1 over A_2 as long as a sufficient amount of component A_1 is present in the aqueous solution in the vicinity of the surface. However, because diffusion is a slow process, consumption of component A_1 will generate a local depletion of A_1 in the vicinity of the crystal layer, so that a switch to an A_2-growth mode may be favored, and so on. This basic mechanism, which is qualitatively similar to the one proposed by Haase et al. (1980), therefore has the potential to generate oscillatory zonation in the crystal.

This paper is organized as follows. In section 2, the basic model is presented. We first discuss the relevant diffusive transport equations and introduce the phenomenological concept of roughness parameter (Ortoleva, 1994). The latter is a necessary ingredient in the generation of oscillatory behavior. We then present the growth rate expressions, with their autocatalytic terms. We simplify the transport equations to a set of ordinary differential equations by using the boundary layer approximation introduced by Wang and Merino (1990, 1992, 1993, 1995). Using adequate scaling parameters, a dimensionless formulation is then presented. In terms of this scaling, we argue that the aqueous solutions are typically highly supersaturated during the growth phase, so that the model can be further simplified. In section 3, we present a linear stability analysis of the autonomous version of the model. It is seen that the system may indeed exhibit Hopf bifurcations, so that oscillatory solutions are obtained. In section 4, we present numerical solutions that confirm the findings of the linear stability analysis. We also examine the more realistic case of time-varying bulk concentrations, thus characterizing the diffusion process through the gel column. Concluding statements and a discussion of the results are presented in section 5. Three appendices complete the paper.

Although the model can be applied to any binary solid solution series grown from aqueous solutions, the $(Ba,Sr)SO_4$ system is specifically used to constraint the model parameters as much as possible.

Table 2. Notation used in our model.

Symbol	Definition
c_i	Concentration of species i in the solid (mol/vol)
D_i	Diffusion coefficient of species i
d_i	Dimensionless diffusion coefficient of species i
H	Length of the diffusion column
l	Boundary layer thickness
L	Surface roughness parameter
m_i	Concentration of species i in solution (mol/vol)
$\hat{m}_i$	Bulk concentration of species i in solution (mol/vol)
m_i^o	Equilibrium concentration of species i in solution (mol/vol)
M_i	Concentrations of species i in the reactants reservoirs (mol/vol)
$p_{1,2}$	Residual probability parameters
t	Time
υ_{BA}, υ_{CA}	Partial molar volume of $BaSO_4$ and $SrSO_4$ in solid $(Ba,Sr)SO_4$, respectively
V_{BA}, V_{CA}	Growth velocity of $BaSO_4$ and $SrSO_4$, respectively
V	Effective crystal growth velocity
x	Position with respect to the crystal-solution interface
x'	Position in the laboratory frame
X	Solid molar fraction of $BaSO_4$
y	Distance between the Ba-Sr reservoir and the crystal
α	Ratio of molar volumes $\upsilon_{CA}/\upsilon_{BA}$
β_{BA}, β_{CA}	Kinetic coefficients of $BaSO_4$ and $SrSO_4$, respectively
β'_{BA}, β'_{CA}	X-independent part of the kinetic coefficients
β	Ratio of kinetic coefficients β'_{CA}/β'_{BA}
γ	Ratio of concentration scale in solution to that in solid
τ	Nucleation time at which crystal growth starts
Λ	Dimensionless roughness parameter

2. MODEL

The notation used in this paper is listed in Table 2. In this section, we present a simple growth model that can be applied to the oscillatory zoning observed in the system $Ba_XSr_{1-X}SO_4$. We are not concerned with the nucleation phase of the crystal, but rather focus on the growth of a previously nucleated crystal from a supersaturated solution. The growth proceeds according to the precipitation reactions:

$$SO_4^{--} + Ba^{++} \rightarrow BaSO_4,$$

$$SO_4^{--} + Sr^{++} \rightarrow SrSO_4.$$

In the following, we use the following symbolic notation: A = SO_4^{--}, B = Ba^{++}, C = Sr^{++}, BA = $BaSO_4$, and CA = $SrSO_4$.

Typically, the observed compositional zoning fronts are approximately parallel to a crystal face. In the vicinity of a planar crystal face and far from the crystal edges, the isopleths are approximately planar. As the distance from a crystal face increases, the isopleths are expected to become progressively more curved, so that sufficiently far from the crystal, the isopleths exhibit an approximate spherical symmetry. As the distance from the crystal increases further, however, the shape of the gel column must be considered, so that the isopleths are expected to become parallel again. A more precise formulation of the diffusion problem would be to consider planar diffusion close to a crystal face, going over to spherical diffusion further from the crystal and back again to planar diffusion for distances of the order of the column width. However, to simplify our model, we will rather reduce the diffusion problem to one spatial dimension, chosen along the direction normal to a crystal face.

2.1. Transport Equations

Let m_i be the concentration (in moles per unit volume) of the ion of species i (i = A, B, or C) in the aqueous solution. Also, let x' be the absolute (laboratory) position of a point in the solution with respect to the position of the nucleated crystal just before growth occurs at time $t = 0$. Then, the evolution of the concentration fields in the aqueous solution is given by the diffusion equation

$$\frac{\partial m_i}{\partial t} = D_i \frac{\partial^2 m_i}{\partial x'^2}, \tag{1}$$

where D_i is the diffusion coefficient of ions of species i in the solution. We will treat this moving boundary problem in the following way: We choose a frame of reference comoving with the growing crystal front, so that $x = 0$ is fixed at the crystal front and the half-space $x > 0$ corresponds to the aqueous solution. The absolute (laboratory) position x' of a point in the solution is thus related to x by

$$x' = x + \int_0^t V(t')\mathrm{d}t', \tag{2}$$

where $V(t)$ is the instantaneous effective growth velocity. In general, the latter depends on the state of the system at the growing front $x = 0$. The diffusion equations thus become

$$\frac{\partial m_i}{\partial t} = D_i \frac{\partial^2 m_i}{\partial x^2} + V \frac{\partial m_i}{\partial x} \tag{3}$$

and are valid for $x \geq 0$. The presence of the second term on the right-hand side is due to the change of coordinate system defined in Eqn. 2.

In a typical experimental setup, the ions in the aqueous solution diffuse in the gel column connecting the two reservoirs. The solution precipitates at the crystal nucleation site, which is typically located close to the middle of the column. Over a length scale comparable to the column length (a few centimeters), the concentrations are therefore not homogeneous and time dependent. However, over a length scale comparable to the crystal dimension (a few hundreds of microns), the concentrations may be assumed uniform in space. We thus define the bulk values of the concentrations as their values at the nucleation site. The bulk values may still be time dependent, however, because of diffusion from the reservoirs. Thus, sufficiently far from the growing front, the concentrations must be equal to their bulk values $\hat{m}_i\,(t)$:

$$m_i\,(\infty,t) = \hat{m}_i\,(t). \tag{4}$$

The initial concentrations are also equal to their bulk values:

$$m_i\,(x,0) = \hat{m}_i\,(0). \tag{5}$$

Finally, the continuity of mass current at the crystal interface ($x = 0$) gives the following boundary condition:

$$D_i \left.\frac{\partial m_i}{\partial x}\right|_{x=0} + [m_i\,(0,t) - c_i\,(t)]V = 0, \tag{6}$$

where $c_i(t)$ denotes the concentration of species i in the solid at the growing front. It is clear from the stoichiometry that

$$c_A = c_B + c_C. \tag{7}$$

We now introduce the solid-phase mole fraction X of $BaSO_4$. If v_{BA} and v_{CA} denote the partial molar volume of $BaSO_4$ and $SrSO_4$ in solid solution $(Ba,Sr)SO_4$ respectively, then we have

$$c_B = \frac{X}{v_{BA}X + v_{CA}\,(1 - X)}, \quad c_C = \frac{1 - X}{v_{BA}X + v_{CA}\,(1 - X)}. \tag{8}$$

A relation between the solid mole fraction and concentrations in the aqueous solution is needed. It can be obtained from the following kinetic arguments. Let V_{BA} and V_{CA} be the growth velocities of $BaSO_4$ and $SrSO_4$, respectively. As shown in Appendix 1, the effective growth velocity of the crystal is simply the sum of the individual growth velocities:

$$V = V_{BA} + V_{CA}. \tag{9}$$

In the stationary growth regime, the $BaSO_4$ mole fraction is proportional to the corresponding precipitation flux (moles per unit area per unit time) G_{BA} (e.g., Wang and Wu, 1995; Ortoleva, 1994; Stauffer, 1976). The latter quantity is written in Eqn. A4 of Appendix 1 as $G_{BA} = V_{BA}v_{BA}$ (and a similar relation for G_{CA}). Thus,

$$X = \frac{G_{BA}}{G_{BA} + G_{CA}} = \frac{V_{BA}/v_{BA}}{V_{BA}/v_{BA} + V_{CA}/v_{CA}}. \tag{10}$$

With appropriate (concentration-dependent) expressions for the growth velocities, the diffusion equation (Eqn. 3) together with the interface boundary condition (Eqn. 6) and Eqn. 8 and 10 constitute a nonlinear system of coupled partial differential equations. Using the approximation scheme described below, we can reduce that system to a set of ordinary differential equations. However, it turns out that this scheme generates no complex solutions (oscillatory or chaotic). We thus consider a supplementary dynamic equation for the composition X. In fact, as Ortoleva (1994, pp. 54, 66) argued, the expression $G_{BA}/(G_{BA} + G_{CA}) - X$ is in general different from zero, since the effects of the roughness of the crystal-solution interface should be taken into account. Ortoleva (1994) introduced a buffer zone between the crystal and the aqueous solution characterized by the length scale L over which the surface roughness is not negligible. Applying the mass flux balance across that interface zone results in a phenomenological dynamic equation for X, which is derived in Appendix 2:

$$\alpha L \frac{dX}{dt} = [X + (1 - X)\alpha]^2[(V_{BA} - X\,(V_{BA} + V_{CA}/\alpha)]. \tag{11}$$

Here, $\alpha = v_{CA}/v_{BA} = 0.89$ is the ratio of solid molar volumes. When the length scale of surface fluctuations is negligible or at steady state, Eqn. 10 is recovered.

2.2. Growth Velocity

Generally, growth of a crystal from a solution may occur according to a combination of various mechanisms. Ignoring convection-induced growth, such mechanisms comprise mainly continuous growth, surface-nucleation growth, and screw-dislocation growth. Approximate expressions for these various growth laws may be found in, e.g., Markov (1996). Studies of the early stages of growth by atomic force microscopy (Pina et al., 2000) suggest that surface-nucleation mechanism plays an important role, at least for small to moderate supersaturation. On the other hand, an investigation of the nucleation and growth of crystals from various 2-2 electrolytes was reported by Nielsen (1969) with an emphasis on barium sulphate growth. It was concluded that for large barium concentrations ($m_B > 0.4$ mM), the growth velocity is proportional to the Ba concentration. For mathematical simplicity, we consider in our model a continuous-growth mechanism, which also results in a growth rate proportional to the concentration, for large supersaturations. In the $(Ba,Sr)SO_4$ growth experiment, the concentrations are expected to first increase as the growth proceeds, as the ions diffuse from the reservoirs through the gel column. Therefore, the assumption of a continuous-growth mechanism is not unreasonable in this case.

In Appendix 3, we generalize the arguments of Markov (1996) to dilute solutions and obtain V_{BA}, the growth velocity of $BaSO_4$, as

$$V_{BA} = \beta_{BA}\,[m_B m_A - (m_B m_A)^o]. \tag{12}$$

Here, $(m_B m_A)^o$ is the product of the equilibrium concentrations of Ba^{++} and SO_4^{--} (for which no growth or dissolution occurs) and β_{BA} is the kinetic coefficient:

$$\beta_{BA} = a_{BA}\,\nu \exp[-\Delta U_{BA}/kT]v_{BA}^2 P_{BA}. \tag{13}$$

In this expression, a_{BA} is the size of a building unit (comparable to the length of a diffusion jump), P_{BA} is the probability of finding a kink site appropriate for $BaSO_4$ attachment on the surface, ν is a frequency factor, and ΔU_{BA} is the energy barrier

for the incorporation of building units into the crystal. Finally, k is Boltzmann's constant, and T is temperature. The growth velocity V_{CA} of $SrSO_4$ can be defined in a similar way.

An estimate of the growth rate of pure $BaSO_4$ can be obtained by using $\Delta U_{BA} = 7$ kcal/mol (Markov, 1996), $T = 300$ K, $P_{BA} \cong 0.1$, $\nu = 6 \times 10^{12}$ Hz, $\upsilon_{BA} = 51.7$ cm^3/mol, $a_{BA} = (\upsilon_{BA}/N_o)^{1/3}$ (N_o being Avogadro's number), and $m_A \cong m_B \cong 10^{-5}$ to 10^{-6} mol/cm^3. We have neglected $(m_B m_A)^o$ compared with $m_A m_B$. We get $V_{BA} \cong 10^{-8}$ cm/s. In the $(Ba,Sr)SO_4$ growth experiments, crystals of size $\sim 10^{-2}$ cm were grown over periods of 400 h, corresponding to an average growth rate of 7×10^{-9} cm/s. These numbers are indeed consistent with our simple theoretical estimate of the growth velocity.

Phenomenologically, the probability P_{BA} of finding a kink site can be expressed (Markov, 1996) as

$$P_{BA} = (a_{BA}/\delta_{BA})^2, \tag{14}$$

where δ_{BA} is the average distance between the kinks, and the exponent 2 comes from the fact that continuous growth occurs on a two-dimensional surface. Growth of $BaSO_4$ units on $BaSO_4$ kink sites is favored over growth of $SrSO_4$ units on a $BaSO_4$ kink site. This is because a lattice misfit always generates a strain energy cost on one hand and because chemical bounding is generally stronger between identical units on the other. Thus, one expects the distance between favorable kink sites for growth of $BaSO_4$ to decrease with increasing mole fraction of $BaSO_4$ on the surface of the crystal. In this way, a $BaSO_4$-rich crystal surface tends to favor the growth of further $BaSO_4$. The simplest relation that takes this constraint into consideration is to assume

$$\frac{a_{BA}}{\delta_{BA}} = \alpha_{BA}\,(X + p_1); \quad \frac{a_{CA}}{\delta_{CA}} = \alpha_{CA}\,(1 - X + p_2), \tag{15}$$

where α_{BA}, α_{CA}, p_1, and p_2 are constants. Physically, ${p_1}^2$ is proportional to the residual probability of finding a favorable kink site for the growth of $BaSO_4$ on a pure $SrSO_4$ surface (i.e., $X = 0$), and p_2 is defined analogously. We redefine the kinetic coefficient as

$$\beta'_{BA} = a_{BA}\,\nu \exp[-\Delta U_{BA}/kT]{\upsilon_{BA}}^2{\alpha_{BA}}^2, \tag{16}$$

with a similar expression for β'_{CA}. The growth velocities thus become

$$\begin{aligned} V_{BA} &= \beta'_{BA}\,[m_B m_A - (m_B m_A)^o](X + p_1)^2; \\ V_{CA} &= \beta'_{CA}\,[m_C m_A - (m_C m_A)^o](1 - X + p_2)^2. \end{aligned} \tag{17}$$

This derivation thus introduces a heuristic but natural way, an autocatalytic mechanism for the continuous growth of a binary solid solution. It turns out that in our model, the nonlinear dependence of the barium mole fraction in the solid on the growth velocities is essential for the generation of oscillatory zoning. This feature is also true for a model of oscillatory zoning discussed by Ortoleva (1994, p. 51) and Haase et al. (1980), in which a dependence of the form $X^2 + a$ (with constant a) was introduced (without physical justification) instead of $(X + p_1)^2$.

In summary, the model is described by the diffusive transport equation (Eqn. 3) with the appropriate boundary conditions (Eqn. 4 and 6) and initial condition (Eqn. 5), together with the relationship between solid concentrations and mole fraction (Eqn. 7 and 8), the growth velocity expressions (Eqn. 9 and 17), and the equation for the evolution of $BaSO_4$ mole fraction in the crystal (Eqn. 11).

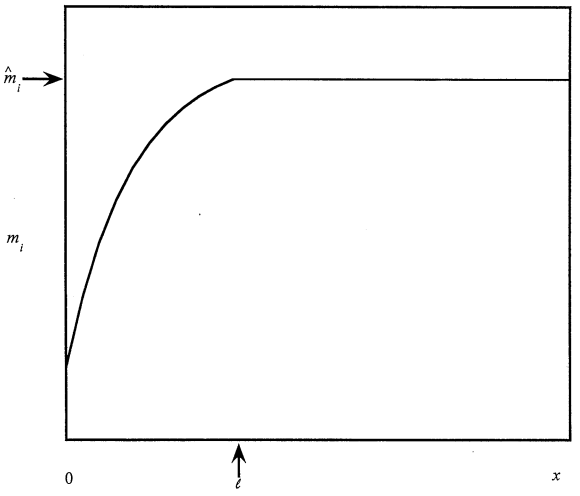

Fig. 2. Schematic representation of the ion concentration field m_i as a function of the position x from the crystal interface in the boundary layer approximation. At a distance l from the interface, the field converges to its bulk value $\hat{m}_i$.

2.3. Boundary Layer Approximation

The diffusion equations (Eqn. 3) are coupled by the nonlinear growth rate term V, which depends on the variables $m_i(0,t)$ and X in a complex manner. Also, these diffusion equations are driven by the nonlinear boundary conditions (Eqn. 6) at the crystal interface $x = 0$. An examination of Eqn. 6 suggests the existence of a length scale l characterizing the distance over which the concentration changes near the crystal interface. Indeed, in the $(Ba,Sr)SO_4$ growth experiments, values of the concentrations range from slightly less than 1 mM to $\sim$100 mM. We will choose a typical concentration scale $\bar{m} = 5$ mM. We also scale the concentrations c_i in the solid by the inverse of the $BaSO_4$ molar volume $\bar{c} = 1/\upsilon_{BA} = 0.019$ mole/cm^3, which must be larger than $\bar{m}$. We let $\bar{V} \sim 10^{-8}$ cm/s be a characteristic growth velocity scale. Moreover, we choose $D_A \sim 10^{-5}$ cm^2/s as a characteristic scale for the diffusion coefficients. Finally, by definition, we scale the concentration derivative at the crystal interface as $\bar{m}/l$. Thus, balancing the scales of the terms in Eqn. 6 implies that the order of magnitude of the boundary layer length l is

$$l = \bar{m} D_A/\bar{V}\bar{c}. \tag{18}$$

A numerical estimate of this order of magnitude gives $l \sim 2$ mm.

The diffusion equation (Eqn. 3) cannot be solved exactly. However, as a first step toward understanding the system behavior, we can reduce the problem to a system of ordinary differential equations in the following way. Since l is large compared to the crystal dimension, we assume that the concentration profiles take the form illustrated in Figure 2, where m_i

reach their asymptotic value $\hat{m}_i$. This assumption about the shape of the concentration profile was also made by Wang and Merino (1990, 1992, 1993, 1995). In fact, the order of magnitude of our estimate for l is compatible with the value given by Wang and Merino (1992) in their model of oscillatory zoning of trace element in calcite grown from supersaturated calcium carbonate solutions containing a cation inhibitor.

We first integrate the diffusion equations (Eqn. 3) across the boundary layer l:

$$\frac{\mathrm{d}}{\mathrm{d}t}\int_0^l m_i\,(x,t)\mathrm{d}x = D_i\left(\left.\frac{\partial m_i\,(x,t)}{\partial x}\right|_{x=l} - \left.\frac{\partial m_i\,(x,t)}{\partial x}\right|_{x=0}\right) + V[m_i\,(l,t) - m_i\,(0,t)]. \quad (19)$$

We approximate the integral on the left-hand side in the following way (Fig. 2):

$$\int_0^l m_i\,(x,t)\mathrm{d}x = \frac{l}{2}\,[m_i\,(0,t) + \hat{m}_i\,(t)], \quad (20)$$

whereas the derivative of the concentration at l is approximately (Fig. 2)

$$\left.\frac{\partial m_i\,(x,t)}{\partial x}\right|_{x=l} = \frac{1}{l}\,[\hat{m}_i\,(t) - m_i\,(0,t)]. \quad (21)$$

We also use the boundary conditions (Eqn. 4) and Eqn. 6 to express the derivative of the concentration at $x = 0$. We finally obtain the transport equations in the boundary layer approximation:

$$\frac{\mathrm{d}m_i\,(0,t)}{\mathrm{d}t} = \frac{2D_i}{l^2}\,[\hat{m}_i\,(t) - m_i\,(0,t)] + \frac{2V}{l}\,[\hat{m}_i\,(t) - c_i\,(t)] - \frac{\mathrm{d}\hat{m}_i\,(t)}{\mathrm{d}t}. \quad (22)$$

With this approximation, the evolution of all quantities depends only on the dynamics at the crystal surface, notwithstanding a possible forcing due to the time dependence of the bulk concentrations. The label $(0,t)$ will thus be omitted in the following.

2.4. Dimensionless Formulation

It is convenient to reduce the model to a dimensionless form. We express the concentrations in the aqueous solution m_i, $(m_i)^{\circ}$, and $\hat{m}_i$ in units of the typical value $\overline{m}$. We also scale the concentrations c_i in the solid by the inverse of the $BaSO_4$ molar volume, $\bar{c} = 1/v_{\mathrm{BA}}$. We scale all growth velocities by the characteristic growth velocity $\overline{V}$. We finally scale the time variable by a time scale

$$\bar{t} = l^2/D_{\mathrm{A}}, \quad (23)$$

chosen to simplify the transport equations (Eqn. 22). We recall that $\alpha = v_{\mathrm{CA}}/v_{\mathrm{BA}}$, and we introduce the following dimensionless parameters:

$$\beta = \beta'_{\mathrm{CA}}/\beta'_{\mathrm{BA}}; \quad \gamma = \overline{m}/\bar{c} << 1; \quad d_{\mathrm{B}} = D_{\mathrm{B}}/D_{\mathrm{A}}; \quad d_{\mathrm{C}} = D_{\mathrm{C}}/D_{\mathrm{A}}; \quad \Lambda = L/\overline{V}\,\bar{t}. \quad (24)$$

In the rest of this paper, a * superscript associated with a variable will denote its scaled dimensionless form. In terms of scaled variables, the diffusive transport equations (Eqn. 22) thus become, using Eqn. 7, 8, 18, and 23,

$$\frac{\mathrm{d}m^*_{\mathrm{A}}}{\mathrm{d}t^*} = 2[\hat{m}^*_{\mathrm{A}}\,(t) - m^*_{\mathrm{A}}] + 2V^*\,[\gamma\hat{m}^*_{\mathrm{A}}\,(t) - 1/(X + \alpha(1 - X))] - \frac{\mathrm{d}\hat{m}^*_{\mathrm{A}}\,(t)}{\mathrm{d}t^*},$$

$$\frac{\mathrm{d}m^*_{\mathrm{B}}}{\mathrm{d}t^*} = 2d_{\mathrm{B}}[\hat{m}^*_{\mathrm{B}}\,(t) - m^*_{\mathrm{B}}] + 2V^*\,[\gamma\hat{m}^*_{\mathrm{B}}\,(t) - X/(X + \alpha(1 - X))] - \frac{\mathrm{d}\hat{m}^*_{\mathrm{B}}\,(t)}{\mathrm{d}t^*}, \quad (25)$$

$$\frac{\mathrm{d}m^*_{\mathrm{C}}}{\mathrm{d}t^*} = 2d_{\mathrm{C}}[\hat{m}^*_{\mathrm{C}}\,(t) - m^*_{\mathrm{C}}] + 2V^*\,[\gamma\hat{m}^*_{\mathrm{C}}\,(t) - (1 - X)/(X + \alpha(1 - X))] - \frac{\mathrm{d}\hat{m}^*_{\mathrm{C}}\,(t)}{\mathrm{d}t^*}.$$

Finally, the equation for the molar composition (Eqn. 11) becomes

$$\frac{\mathrm{d}X}{\mathrm{d}t^*} = \frac{1}{\alpha\Lambda}\,[X + (1 - X)\alpha]^2[V^*_{\mathrm{BA}} - X(V^*_{\mathrm{BA}} + V^*_{\mathrm{CA}}/\alpha)]. \quad (26)$$

Here, the scaled growth velocities are given by

$$V^*_{\mathrm{BA}} = [m^*_{\mathrm{B}}m^*_{\mathrm{A}} - (m^*_{\mathrm{B}}m^*_{\mathrm{A}})^{\circ}](X + p_1)^2,$$
$$V^*_{\mathrm{CA}} = \beta[m^*_{\mathrm{C}}m^*_{\mathrm{A}} - (m^*_{\mathrm{C}}m^*_{\mathrm{A}})^{\circ}](1 - X + p_2)^2, \quad (27)$$
$$V^* = V^*_{\mathrm{BA}} + V^*_{\mathrm{CA}}.$$

With l of the order of 2 mm, Eqn. 23 gives a time scale $\bar{t} \sim 5 \times 10^3$ s. In turn, this choice of scaling corresponds to a spatial scale for the zoning (see Eqn. 2) of the order of $\lambda \sim \overline{V}\,\bar{t} \sim 0.5$ μm, which is consistent with the scale of the observed zoning.

2.5. Equilibrium Concentration Products

The equilibrium concentration products appear in the relation defining the solubility products of the pure end-members $K_{\mathrm{BA}} = 10^{-9.98}$ M^2 and $K_{\mathrm{CA}} = 10^{-6.63}$ M^2:

$$([A][B])^{\circ} = \gamma_A\gamma_B\,(m_{\mathrm{A}}m_{\mathrm{B}})^{\circ} = K_{\mathrm{BA}}\gamma_{\mathrm{BA}}X;$$
$$([A][C])^{\circ} = \gamma_A\gamma_C\,(m_{\mathrm{A}}m_{\mathrm{C}})^{\circ} = K_{\mathrm{CA}}\gamma_{\mathrm{CA}}\,(1 - X). \quad (28)$$

Here, ([A] [B])$^{\circ}$ and ([A] [C])$^{\circ}$ are the product of the equilibrium activities (in molar units) of the corresponding ions, and γ_i is the activity coefficient of component i in the solid solution (i = BA,CA) or in the aqueous solution (i = A,B,C). As argued by Prieto et al. (1993, 1997), the solid solution may be considered ideal for many practical purposes, so that $\gamma_{\mathrm{AB}} = \gamma_{\mathrm{AC}} = 1$. For calculating the other activity coefficients, the Debye-Hückel formula can be used together with a solvation model

(Prieto et al., 1990, 1993). However, our conclusion does not change if we consider the aqueous solution as ideal. For the sake of simplicity, we set all other activity coefficients equal to unity. From Eqn. 28, it is seen that the equilibrium concentration products are approximately given by $\sqrt{K_{BA}}$ and $\sqrt{K_{CA}}$ and are much smaller than typical concentration products. We can therefore neglect these terms in the growth velocity expressions of Eqn. 27. Direct measurements of the concentrations (Prieto et al., 1990, 1993) suggest that the crystals typically grow in a strongly supersaturated environment, so that our approximation is also appropriate when the nonideality of the aqueous solution is taken into account.

3. LINEAR STABILITY ANALYSIS

To investigate the dynamic properties of the model, it is useful to perform a linear stability analysis on the autonomous version of Eqn. 25 and 26, i.e., with constant bulk concentrations $\hat{m}_i$. Setting the right-hand side of Eqn. 25 and 26 equal to 0 and using Eqn. 27 result in a set of four nonlinear equations, to be solved for the steady states (fixed points) m_i^{*s}, X^s. For given values of the residual probabilities p_i and the roughness parameter Λ, it is straightforward to find the fixed points numerically. It turns out that there always exists at least one fixed point (denoted FP1 below) for all values of p_i and Λ. Moreover, for sufficiently small values of p_i, the system exhibits multistability, so that three fixed points coexist (FP1, FP2, and FP3). The stability of these fixed points is investigated by assuming perturbations of the system of the form

$$\begin{pmatrix} m_i^* \\ X \end{pmatrix} = \begin{pmatrix} m_i^{*s} \\ X^s \end{pmatrix} + \begin{pmatrix} \delta_i \\ \delta_X \end{pmatrix} \exp(\omega t^*) \qquad (29)$$

about a given fixed point. Here, ω is the time-eigenvalue, and δ_i and δ_X are small perturbation amplitudes. The time-eigenvalues are found by setting the determinant of the 4-by-4 matrix $\mathbf{J}$-$\omega\mathbf{1}$ equal to 0, where $\mathbf{J}$ is the Jacobian of the system (Eqn. 25 and 26), and $\mathbf{1}$ is the 4-by-4 identity matrix.

In our calculations, the terms proportional to γ in Eqn. 25 were neglected. The parameter β was set equal to 1. Figure 3a illustrates a typical stability phase diagram in the parameter-space (Λ, p_1) pertaining to the fixed point FP1, for a particular choice of the bulk concentrations, and for $p_1 = p_2$. In such diagrams, the lines separate regimes that exhibit the various stability behaviors of that fixed point. In the regions denoted SN (stable node), all four eigenvalues are real and negative. The fixed point FP1 is therefore stable and corresponds to a crystal evolving toward a constant composition. In the region SF (stable focus), at least two eigenvalues (mutually complex-conjugate) have nonzero imaginary parts, but all have negative real parts. This corresponds to a stable fixed point that supports damped oscillations. However, in the region denoted UF (unstable focus), two eigenvalues have nonzero imaginary parts but positive real parts. This regime corresponds to an unstable fixed point that has the potential to generate limit cycle solutions, i.e., oscillatory zoning. On the line separating the UF regime from the SF regime, the real parts of the eigenvalues become zero, whereas the imaginary parts are not. Thus, this line defines the locus of the Hopf bifurcations. Finally, the region denoted S^2 (saddle) corresponds to an unstable fixed point with two real positive eigenvalues.

For values of p_i smaller than $p_b \cong 0.1275$ (indicated by the dotted line in the figure), a saddle node bifurcation generates two new fixed points FP2 and FP3, one of them being unstable. Figure 3b illustrates the bifurcation diagram $X^s(p_1)$ for all three fixed point branches in the small-p_1 region for a particular choice of Λ and of the bulk concentrations and for $p_2 = p_1$. The label S^1 (saddle) denotes an unstable fixed point with one real positive eigenvalue. The system therefore exhibits bistability in this regime, so that the large-time crystal composition is controlled by the initial values. The existence of the bistability regime does not depend on the value of the roughness parameter Λ, since this parameter does not appear in the determination of the fixed points.

For larger bulk concentrations, the topological structure of the FP1 stability diagram is similar to Figure 3a. There are some quantitative differences, however. For instance, the rightmost limits of instability (S^2 and UF regions) occur at larger values of Λ as the $\hat{m}_i^*$ increase. Also, as $\hat{m}_i^*$ increase, the small-p_i limit of these unstable regions becomes smaller, and their large-p_i limit increases. These features are illustrated in Figure 3c, in which a stability phase diagram for FP1 is given in the $\hat{m}_A^*$, p_1 parameter space for a fixed value of Λ, $p_2 = p_1$, and $\hat{m}_B^* = \hat{m}_C^* = \hat{m}_A^*$. In consequence, the regime for which the fixed point FP1 is unstable is larger when the bulk concentrations are larger. Thus, the generation of oscillatory-zoned solutions is more probable for larger bulk concentrations.

4. NUMERICAL SOLUTIONS

In this section, we verify the findings of the linear stability analysis and illustrate the nature of the solutions in the unstable regimes by exhibiting various numerical solutions to the system (Eqn. 25 to 27; neglecting the terms proportional to $\gamma \ll 1$). The numerical solutions were straightforwardly obtained by a Runge-Kutta fourth-order algorithm. Once the concentrations as a function of time were determined, the growth velocity V^* was calculated from Eqn. 27. This was in turn numerically integrated (Eqn. 2) to find the laboratory space coordinate x'^* (scaled by the factor $\lambda = \bar{V}\bar{t}$). We thus obtained spatial profiles of the crystal Ba composition X from the crystal core.

4.1. Constant Bulk Concentrations

In this set of numerical experiments, the bulk concentrations $\hat{m}_i^*$ were kept constant in time. This reflects the situation discussed in section 3. Figure 4 illustrates the typical composition profiles obtained for the case corresponding to Figure 3, with Λ fixed at 0.01 (which corresponds to $L \sim 5$ nm) and various $p_1 = p_2$. In Figure 4a, $p_1 = 0.5$. In terms of the linear stability analysis, this corresponds to the (unique) fixed point being a stable focus. The solution indeed exhibits a decaying oscillatory profile that evolves to a constant value. In Figure 4b, p_1 is reduced to 0.44, which corresponds to a point in the unstable focus region of the stability phase diagram. The solution exhibits an oscillatory zoning that is strictly periodic and with a poor spectral content. The wavelength of the oscillation is 0.66 dimensionless units, which corresponds to 0.3 μm. The spatial scale of the oscillations is thus of the same order of magnitude as the observed ones. As p_1 is reduced further to 0.2 (Fig. 4c),

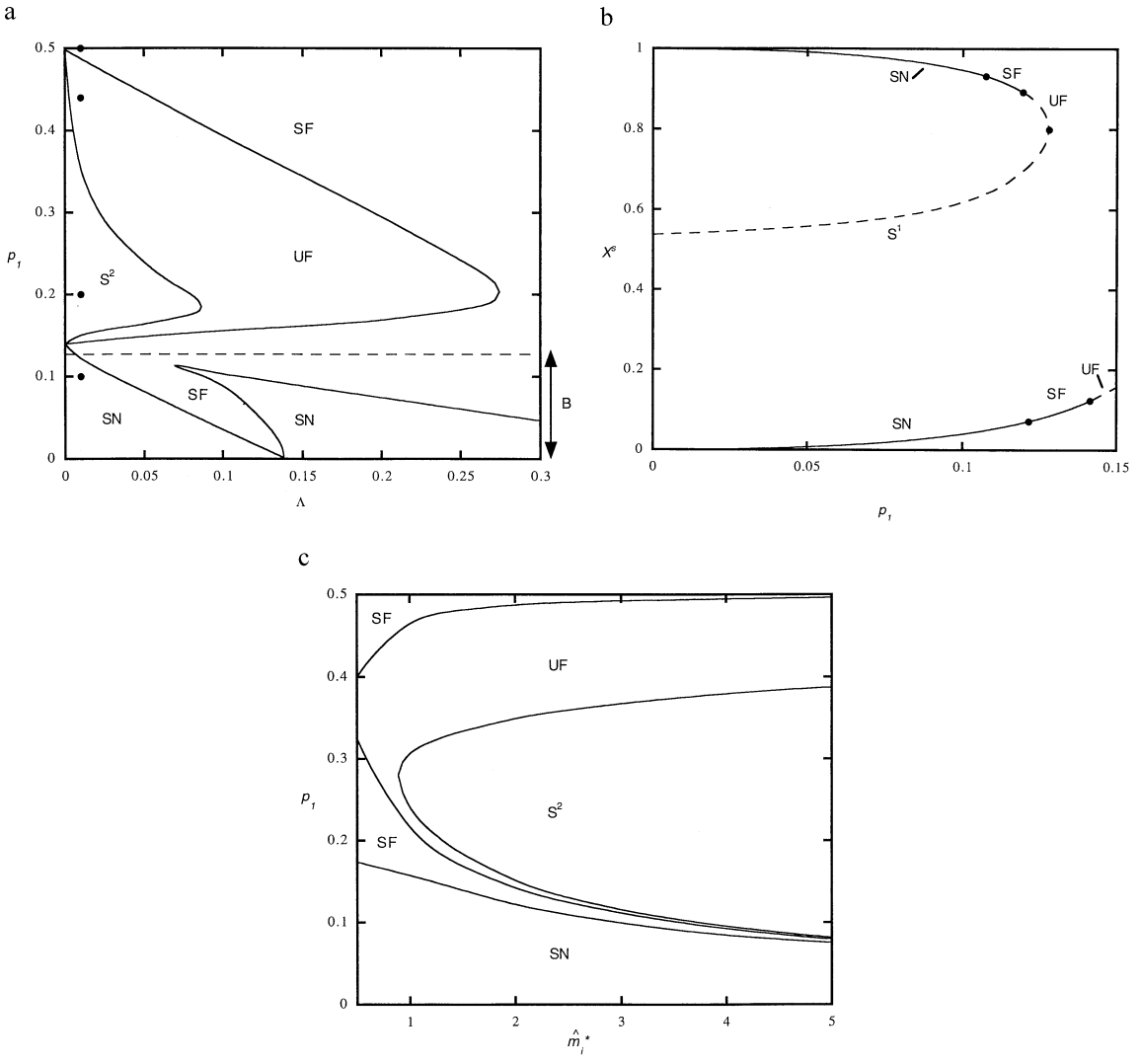

Fig. 3. (a) Stability phase diagram for our model with constant bulk concentrations $\hat{m}_i^* = 2$ and $p_1 = p_2$ in the (Λ, p_1) parameter space. The other parameters were chosen as $\alpha = 0.89$, $\beta = 1$, $d_B = 0.79$, and $d_C = 0.74$. SF denotes the stable focus area, UF denotes the unstable focus domain, S^2 represents a saddle region (with two real positive eigenvalues), and SN corresponds to a stable node. The bistability region B is indicated by the vertical arrow on the right of the diagram. The four black dots along the line $\Lambda = 0.01$ correspond from top to bottom to the cases illustrated in Figures 4a to 4d, respectively. (b) Bifurcation diagram giving the steady state branches X^s as a function of p_1, for $\Lambda = 0.01$. All other values are as in (a). The steady state branches are classified as SF (stable focus), UF (unstable focus), SN (saddle node), and S^1 (saddle with one real positive eigenvalue). (c) Stability phase diagram with constant $\Lambda = 0.01$, $p_1 = p_2$ and $\hat{m}_A^* = \hat{m}_B^* = \hat{m}_C^*$ in the ($\hat{m}_A^*$, p_1) parameter space. All other parameters are as in (a).

the system crosses over to the saddle regime of the stability diagram. Here, the composition profile is again strictly periodic, but the spectral content of the oscillation is much richer: The concentration changes abruptly from small values to large ones. Again, the wavelength of the oscillations (0.9 μm) is of the same order of magnitude as the observations. Finally, Figure 4d illustrates bistability: here, p_1 is smaller than p_b, and two stable fixed points coexist. No oscillatory profiles are possible in this regime, at least for constant boundary conditions. However, in an uncontrolled natural environment, fluctuations in the bulk concentrations could lead to noise-induced bimodal zoning patterns if the fluctuation amplitudes are sufficiently large (Holten et al., 2000).

4.2. Variable Bulk Concentrations

In reality, the ions in the aqueous solution diffuse through the gel column from the reactants reservoirs. Therefore, the value $\hat{m}_i$ of the concentrations at the nucleation site is not constant in time but changes according to the solution of a diffusion equation. It is possible to relate these concentrations to the known concentrations of the mother solutions in the reservoirs. Let y denote the distance from the $BaCl_2$ and $SrCl_2$ reservoir to the crystal growth site. Then, $\hat{m}_i$ (with i = B,C) obeys the (dimensionalized) diffusion equation

$$\frac{\partial \hat{m}_i}{\partial t} = D_i \frac{\partial^2 \hat{m}_i}{\partial y^2}. \tag{30}$$

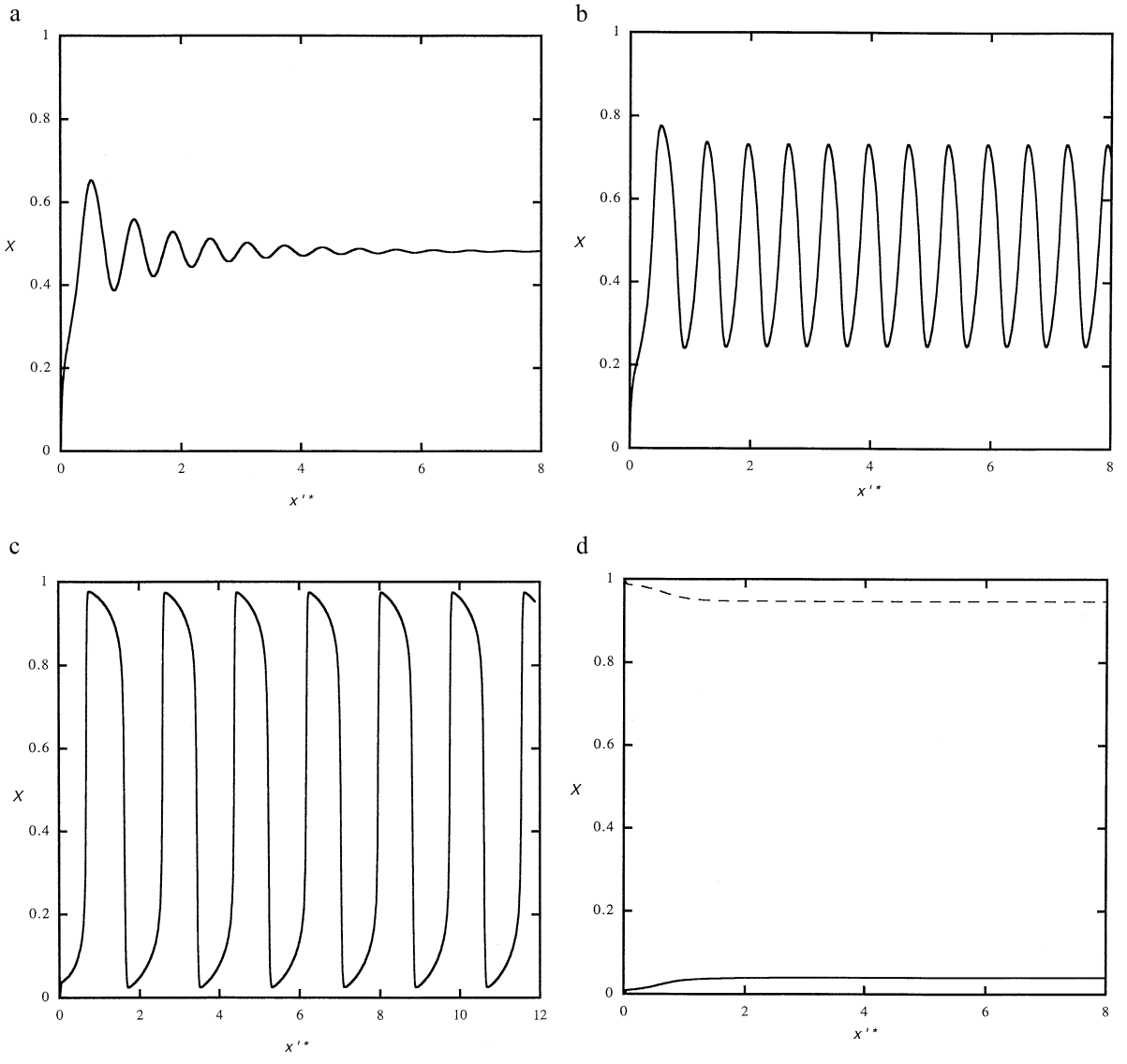

Fig. 4. Crystal barium sulphate composition X as a function of the scaled position from the core of the crystal x'^* for $\alpha = 0.89$, $\beta = 1$, $d_B = 0.79$, $d_C = 0.74$, all $\hat{m}_i^* = 2$, $\Lambda = 0.01$, and various $p_1 = p_2$. The initial concentrations were $m_i^*(0) = \hat{m}_i^*$ *(a)* $p_1 = 0.5$ and $X(0) = 0$; (b) $p_1 = 0.44$ and $X(0) = 0$; (c) $p_1 = 0.2$ and $X(0) = 0$; (d) $p_1 = 0.1$ and $X(0) = 0$ (continuous line) or $X(0) = 1$ (dashed line). The latter case illustrates bistability.

Similarly, $\hat{m}_A$ obeys the diffusion equation

$$\frac{\partial \hat{m}_A}{\partial t} = D_A \frac{\partial^2 \hat{m}_A}{\partial y'^2}, \tag{31}$$

where $y' = H - y$ is the distance from the Na_2SO_4 reservoir to the crystal growth site, with $H = 28$ cm being the length of the gel column. Assuming that the reservoirs are inexhaustible and that H is large compared to the diffusion length $\sqrt{D_i t}$, the solution to Eqn. 30 and 31 reads

$$\hat{m}_{B,C}(t) = M_{B,C} \operatorname{erfc}[y/2\sqrt{D_{B,C}(t+\tau)}], \tag{32}$$

$$\hat{m}_A(t) = M_A \operatorname{erfc}[(H-y)/2\sqrt{D_A(t+\tau)}], \tag{33}$$

where M_i is the known concentration of component i in the reservoir and erfc is the complementary error function. Here, $t > 0$ corresponds to the crystallization process of interest, so that the origin of time is shifted by the nucleation time τ, which is itself measured from the moment when the reservoir solutions begin their diffusion process through the gel column. Although analytical solutions are available for finite H, the solution does not differ appreciably from Eqn. 32 and 33 for sufficiently small times. Also, direct measurements of the temporal variations in concentrations as a function of position (Prieto et al., 1990) were performed for reservoir concentrations $M_A = M_B = 0.5$ mol/L. The results suggest that Eqn. 32 and 33 are good representations of the concentration fields for large reservoir concentrations as long as the time is sufficiently short for the reservoirs to be considered unexhausted. The time

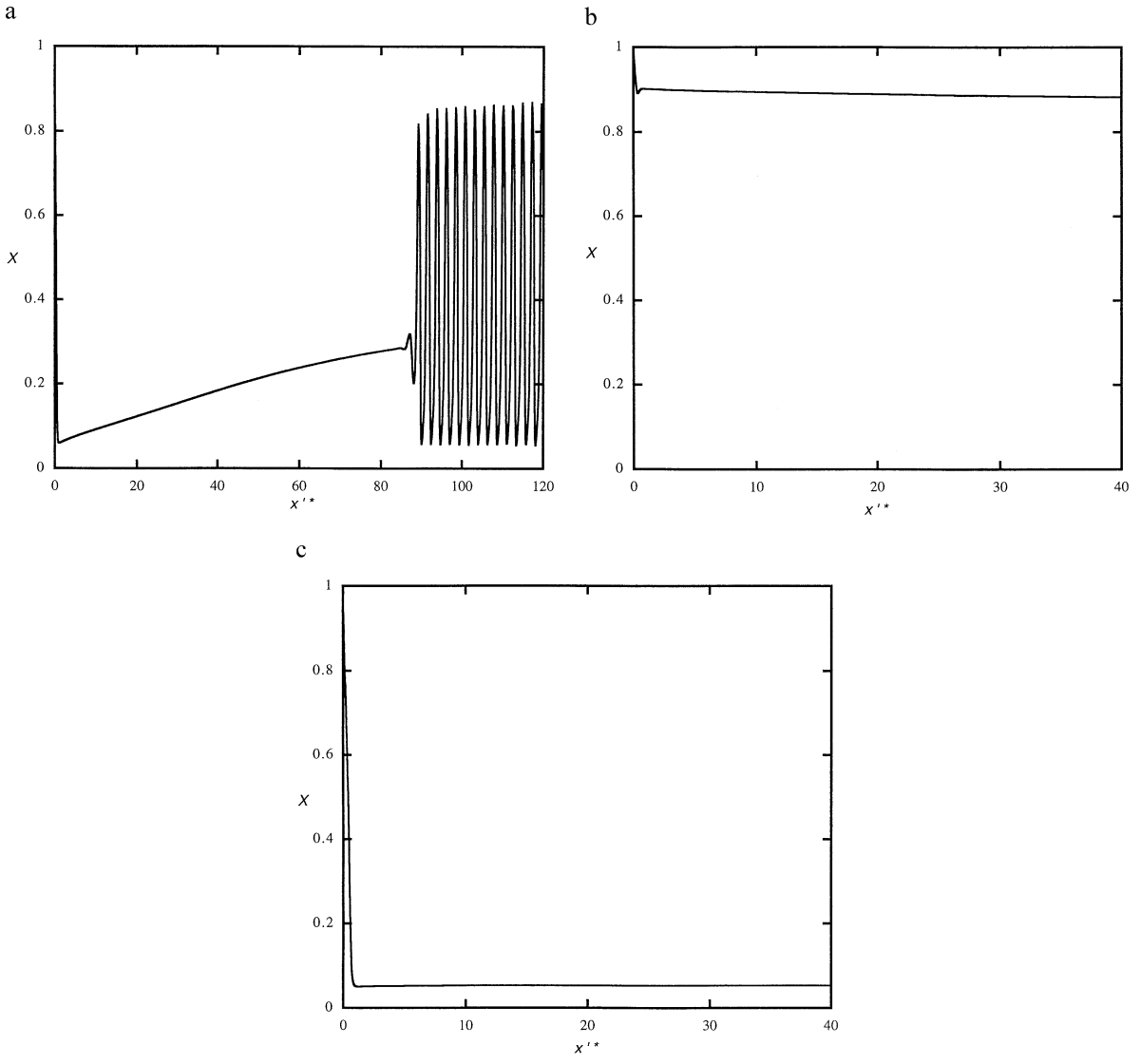

Fig. 5. Crystal barium sulphate composition X as a function of the scaled position from the core of the crystal x'^* for $\alpha = 0.89$, $\beta = 1$, $d_B = 0.79$, $d_C = 0.74$, $\Lambda = 0.05$, $p_1 = 0.2$, and $p_2 = 0.4$. The initial composition was $X(0) = 1.0$, and the bulk compositions varied according to the solution of the diffusion equations (Eqn. 32 and 33). (a) $M_A = 0.5$ mol/L, $M_B = M_C = 0.3$ mol/L, $\tau = 336$ h, $y = 12.3$ cm; (b) $M_A = 0.1$ mol/L, $M_B = 0.3$ mol/L, $M_C = 0.1$ mol/L, $\tau = 576$ h, $y = 15.8$ cm; (c) $M_A = 0.1$ mol/L, $M_B = M_C = 0.5$ mol/L, $\tau = 384$ h, $y = 13.6$ cm.

required for significant reservoir depletion is typically much larger than the crystallization times of interest.

In Prieto et al. (1993), we find direct measurements of the Ba^{++} and Sr^{++} concentrations at the site and time of nucleation of the crystal for various reservoir concentrations. The nucleation times are also known. We can therefore estimate the position y of the nucleation site from Eqn. 32 and the concentration of SO_4^{--} at the nucleation site from Eqn. 33. We thus have all the necessary information to simulate the crystallization process during which the aqueous solution diffuses in the gel column.

Figure 5 presents the computed Ba crystal molar fraction as a function of the distance from the core when the bulk concentrations are chosen according to Eqn. 32 and 33. Figure 5a illustrates the case $M_A = 0.5$ mol/L, $M_B = M_C = 0.3$ mol/L for which oscillatory zoning was experimentally observed (case 3 in Table 1). The numerical solution is qualitatively consistent with this fact. We note also that compared to the case in which the bulk concentrations are constant, the crystal reaches an oscillatory regime much further from the core. This corresponds more closely to the distance for which the large-amplitude zoning is exhibited in the profiles illustrated by Prieto et al. (1993). This behavior can be explained in terms of stability phase diagrams similar to those in Figure 3a, except that the boundaries between the stability regimes evolve in time as the bulk concentrations increase during diffusional transport. For small times, the bulk concentrations are small, and the stable node regime (analogous to the zone in the bottom right corner of Fig. 3a) extends over a large portion of the phase diagram. The corresponding stable fixed point is strontium-rich. As the salt diffuses through the column, the bulk concentration increases and, as noted in section 3, the stable node region

occupies a much smaller portion of the phase diagram, whereas the unstable focus and saddle regions grow rightward from the left. This is why the numerical solution exhibits a sudden oscillatory zoning as time increases.

The case $M_A = 0.1$ mol/L and $M_B = M_C = 0.3$ mol/L from Table 1 is illustrated in Figure 5b. Here, in agreement with the observed profile, barite crystals are obtained. In reference to the stability phase diagram, this is explained by the fact that the initially small bulk concentrations do not increase sufficiently with diffusion to induce a transition in an instability region. The stable fixed point here is indeed barium-rich. Figure 5c illustrates the case $M_A = 0.1$ mol/L and $M_B = M_C = 0.5$ mol/L, for which the observed profile is described by the succession Ba-rich, Sr-rich, Ba-rich. The numerical solution captures the first Ba-rich zone and the Sr-rich zone. In contrast to the observations, the solution then stays at a more or less constant Sr composition level.

We have performed many numerical experiments for various choices of the roughness parameter Λ and the residual probabilities p_i. It turns out that the cases 1 to 4 reported in Table 1 generate oscillatory zoning for a relatively large range of parameter values. Case 5 evolves toward a Ba-rich profile or an Sr-rich profile (as in Fig. 5c) depending on the choice of the parameter values. No oscillatory zoning was found. Case 6 is similar to case 5, although oscillatory zoning occurs for a very small range of parameter values. Case 7 corresponds to a barium-rich profile for all values of these parameters, as in Figure 5b. Finally case 8 corresponds most of the time to an Sr-rich profile, with oscillatory zoning occurring for a small range of parameter values.

5. DISCUSSION AND CONCLUSIONS

In this paper, we have presented a model for the growth of $(Ba,Sr)SO_4$ crystals from aqueous solutions diffusing through a gel column. The main objective of this investigation is to better understand the formation of the oscillatory zoning observed in such crystals. Following Ortoleva (1994, p. 54), we first considered a general growth-diffusion process coupled to a kinetically defined solid solution composition X. Through the application of a boundary layer approximation, we have reduced the model to a set of ordinary differential equations. We have used a continuous growth mechanism with autocatalytic terms. The model shows a rich dynamical behavior, including bistability and periodic composition profiles with wavelengths comparable to the observed ones.

We have also considered the more realistic situation in which the concentrations of the reactants in the aqueous solution are actually changing in time as a result of their diffusion in the gel column from the reservoirs. The dynamical behavior obtained in the numerical solution can be understood in terms of the evolution of the boundaries in the stability phase diagram.

The model parameters are linked to the reactant concentrations in the reservoirs, and comparisons of our modeled composition profiles to actual experiments (such as those reported by Prieto et al., 1993) can be made, at least qualitatively. Thus, the presence of oscillatory zoning in our numerical solutions for the first three cases reported in Table 1 is consistent with the observations. The absence of oscillatory zoning in the last four cases is also consistent with our numerical finding. The barium-rich profile of case 7 is completely consistent with our model. As a rule of thumb, the larger the final concentrations, the more probable are oscillatory profiles. Thus, larger reservoir concentrations and longer growth times (such as when the nucleation time is small) favor oscillatory zoning.

However, the experimentally observed composition profiles characterized by the succession Ba-rich to Sr-rich and to Ba-rich again (cases 4, 5, 6, and 8 in Table 1) have only been found once in our model (corresponding to case 6), and this is for a small range of the values of Λ and p_i. Finally, the profile characterized by the succession Sr-rich to Ba-rich (case 8) has not been found in our numerical solutions. Since the last four cases correspond to small reservoir concentrations, it is possible that the reservoirs become significantly exhausted during the crystallization, so that the bulk concentrations actually decrease and Eqn. 32 and 33 are no longer valid. More realistic solutions to the diffusion equations should be used in such cases.

Extensions of our model are required to account for subtler spatial dependence of the concentration fields near the crystallization front. The next step is to numerically solve the full coupled partial differential equation (Eqn. 3). In fact, preliminary results suggest that the system dynamics in that case is qualitatively similar to that of the reduced version explored in this paper: Bistability, unstable focus, and saddle points leading to oscillatory solutions were also found in the numerical solutions of Eqn. 3. A more complete study of the solutions of Eqn. 3 is currently being undertaken.

We have also considered other growth models, such as screw dislocation mechanism and surface nucleation mechanism. No oscillatory solutions were obtained when using approximate growth velocities expressions corresponding to these mechanisms (Nielsen, 1969; Markov, 1996) in Eqn. 22. However, these growth velocities are difficult to model properly. In any case, more complex growth mechanisms should be considered, such as a combination of continuous growth and growth by surface nucleation.

Our model contains many control parameters, and the apparent agreement between our results and many experimental features does not prove that the self-organization mechanism considered here is the one actually operating in the $(Ba,Sr)SO_4$ system. Nevertheless, given the various assumptions, approximations, and estimates used in the calculations, we believe that our model constitutes an interesting step toward understanding oscillatory zoning in solid solutions grown from aqueous solution. For instance, such models could be applied to systems that exhibit oscillatory zoning characterized by an abrupt transition from one end-member to the other. Our model also presents the possibility that a source of external fluctuations ("noise") could induce transitions from one end-member to the other in the regime in which the system is deterministically bistable (see, e.g., Jamtveit, 1991).

Acknowledgments—We acknowledge fruitful discussions with A. Putnis and C. Pina. Ivan L'Heureux's research was supported by a grant from the Natural Sciences and Engineering Research Council of Canada. He also acknowledges fruitful discussion with S. Katsev. The authors are also grateful to the referees (J. Cartwright from Granada, A. Provost from Clermont-Ferrand, and Y. Wang from Sandia Labs, Carlsbad, New Mexico) for suggesting constructive improvements to the manuscript.

Associate editor: E. Merino

REFERENCES

Allègre C. J., Provost A., and Jaupart C. (1981) Oscillatory zoning: A pathological case of crystal growth. *Nature* **294,** 223–228.

Cross M. C. and Hohenberg P. C. (1993) Pattern formation outside of equilibrium. *Rev. Mod. Phys.* **65,** 851–1112.

Haase C. S., Chadam J., Feinn D., and Ortoleva P. (1980) Oscillatory zoning in plagioclase feldspar. *Science* **209,** 272–274.

Holten T., Jamtveit B., Meakin P., Cortini M., Blundy J., and Austrheim H. (1997) Statistical characteristics and origin of oscillatory zoning in crystals. *Am. Mineral.* **82,** 596–606.

Holten T., Jamtveit B., and Meakin P. (2000). Noise and oscillatory zoning of minerals. *Geochim. Cosmochim. Acta* **64,** 1893–1904.

Jamtveit B. (1991) Oscillatory zonation patterns in hydrothermal grossular-andradite garnet: Nonlinear dynamics in regions of immiscibility. *Am. Mineral.* **76,** 1319–1327.

Katsev S. and L'Heureux I. (2000). Impact of environmental noise on oscillatory pattern formation in crystal growth: Plagioclase feldspar. *Phys. Rev. E.* **61,** 4972–4979.

L'Heureux I. (1993) Oscillatory zoning in crystal growth: A constitutional undercooling mechanism. *Phys. Rev. E.* **48,** 4460–4469.

L'Heureux I. and Fowler, A.D. (1996) Isothermal constitutive undercooling as a model for oscillatory zoning in plagioclase. *Can. Mineral.* **34,** 1137–1147.

Markov I.V. (1996) *Crystal Growth for Beginners*. World Scientific, Singapore.

Nielsen A. (1969) Nucleation and growth of crystals at high supersaturation. *Kristall und Technik* **4,** 17–38.

Ortoleva P. (1994) *Geochemical Self-Organization*. Oxford University Press, New York.

Pearce T. H. and Kolisnik A. M. (1990) Observations of plagioclase zoning using interference imaging. *Earth Sci. Rev.* **29,** 9–26.

Pearce T. H., Russell J. K., and Wolfson I. (1987) Laser-interference and Nomarski interference imaging of zoning profiles in plagioclase phenocrysts from the May 18, 1980, eruption of Mount St. Helens, Washington. *Am. Mineral.* **72,** 1131–1143.

Pina C. M., Enders M., and Putnis A. (2000). The composition of solid solutions crystallizing from aqueous solutions: The influence of supersaturation and growth mechanisms. *Chem. Geol.* **168,** 195–210.

Prieto M., Putnis A., and Fernandez-Diaz L. (1990) Factors controlling the kinetics of crystallization: Supersaturation evolution in a porous medium. Application to barite crystallization. *Geol. Mag.* **127,** 485–495.

Prieto M., Putnis A., and Fernandez-Diaz L. (1993) Crystallization of solid solutions from aqueous solutions in a porous medium: Zoning in $(Ba,Sr)SO_4$. *Geol. Mag.* **130,** 289–299.

Prieto M., Fernandez-Gonzalez A., Putnis A., and Fernandez-Diaz L. (1997) Nucleation, growth, and zoning phenomena in crystallizing $(Ba,Sr)CO_3$, $Ba(SO_4,CrO_4)$, $(Ba,Sr)SO_4$, and $(Cd,Ca)CO_3$ solid solutions from aqueous solutions. *Geochim. Cosmochim. Acta* **61,** 3383–3397.

Putnis A., Fernandez-Diaz L., and Prieto M. (1992) Experimentally produced oscillatory zoning in the $(Ba,Sr)SO_4$ solid solution. *Nature* **358,** 743–745.

Reeder R. J., Fagioli R. O., and Meyers W.J. (1990) Oscillatory zoning of Mn in solution-grown calcite crystals. *Earth Sci. Rev.* **29,** 39–46.

Shore M. and Fowler A. D. (1996) Oscillatory zoning in minerals: A common phenomenon. *Can. Mineral.* **34,** 1111–1126.

Stauffer D. (1976) Kinetic theory of two-component ("hetero-molecular") nucleation and condensation. *J. Aerosol Sci.* **7,** 319–333.

Wang Y. and Merino E. (1990) Self-organizational origin of agates: Banding, fiber twisting, composition, and dynamic crystallization model. *Geochim. Cosmochim. Acta* **54,** 1627–1638.

Wang Y. and Merino E. (1992) Dynamic model of oscillatory zoning of trace elements in calcite: Double layer, inhibition, and self-organization. *Geochim. Cosmochim. Acta* **56,** 587–596.

Wang Y. and Merino E. (1993) Oscillatory magma crystallization by feedback between the concentrations of the reactant species and mineral growth rates. *J. Petrol.* **34,** 369–382.

Wang Y. and Merino E. (1995) Origin of fibrosity and banding in agates from flood basalts. *Am. J. Sci.* **295,** 49–77.

Wang J.-H. and Wu J.-P. (1995) Oscillatory zonation of minerals and self- organization in silicate solid-solution systems: A new nonlinear dynamic model. *Eur. J. Mineral.* **7,** 1089–1100.

APPENDIX 1

Effective Growth Velocity

In this appendix, we show that the effective growth velocity is given by Eqn. 8:

$$V = V_{\mathrm{BA}} + V_{\mathrm{CA}}. \tag{A1}$$

Let N_i be the total number of moles of species i in the crystal and v_i be the partial molar volume of species i (i = $BaSO_4$ or $SrSO_4$). The volume Ω of the crystal is thus

$$\Omega = \sum_i N_i v_i. \tag{A2}$$

As a result of the growth in the direction normal to the crystal-solution interface, the solid volume increases at a rate

$$\frac{\mathrm{d}\Omega}{\mathrm{d}t} = \sum_i \frac{\mathrm{d}N_i}{\mathrm{d}t} v_i = SV, \tag{A3}$$

where S is the area of the interface, and V is the effective growth velocity. We have assumed here that the partial molar volumes are independent of the concentrations in the solid phase, which is the case when the solid solution is considered ideal. But,

$$\frac{\mathrm{d}N_i}{\mathrm{d}t} = S\,\frac{V_i}{v_i}, \tag{A4}$$

where V_i is the growth velocity of species i. Therefore,

$$SV = S\sum_i V_i, \tag{A5}$$

and Eqn. A1 results.

APPENDIX 2

Evolution of the Solid Phase Composition

In this appendix, we derive Eqn. 11 for the evolution of the local $BaSO_4$ composition (molar fraction) in the solid X. We adapt here the arguments of Ortoleva (1994, p. 54).

As mentioned in section 2.1, the composition X can be assumed to be proportional to the $BaSO_4$ precipitation flux G_{BA}, so that its bulk value can be written as Eqn. 10. However, this approach does not take into account the fact that the crystal surface is not flat but may be microscopically rough.

We consider a slab of thickness $2L$ and surface S centered on the average position of the solid interface (at $x = 0$). L (formally defined below) is of the order of the length scale of the crystal surface fluctuations and must be chosen much smaller than the characteristic length associated with the macroscopic crystal zoning. Thus, the slab describes a buffer zone between the aqueous solution and the crystal proper. We can formally define the composition X in the slab as the ratio of appropriate microscopic volume averages:

$$X = \frac{\displaystyle\int_{\mathrm{slab}} \mathrm{d}^3 r\,\theta(\mathbf{r},t)\,p_{BA}(\mathbf{r},t)}{\displaystyle\int_{slab} \mathrm{d}^3 r\,\theta(\mathbf{r},t)}, \tag{A6}$$

where $\theta(\mathbf{r},t)$ is the characteristic function at position $\mathbf{r}$ and time t, which is equal to unity if $\mathbf{r}$ is in the solid phase and zero otherwise. In Eqn. A6, p_{BA} is the microscopic probability that the formula unit at $\mathbf{r}$ is $BaSO_4$. We introduce the local number of moles of all units per unit solid volume:

$$\rho = \frac{1}{v_{BA} X + (1 - X) v_{CA}}. \quad \text{(A7)}$$

Then, ρ times the numerator of Eqn. A6 is the number of $BaSO_4$ units in the slab. After a time Δt, the change in this number of $BaSO_4$ units must be balanced by the number of $BaSO_4$ units incoming to the slab from the aqueous solution ($SG_{BA}\,\Delta t$) and by the number of $BaSO_4$ units integrated in the crystal on the other side of the slab, the latter being proportional to $X\,\Delta t$. Dividing by Δt and going to the limit $\Delta t \to 0$ result in the following mole-balance equation:

$$\frac{d}{dt}\,\rho \int_{slab} d^3x\,\theta(\mathbf{r},t)\,p_{BA}(\mathbf{r},t) = SG_{BA} - SX\,(G_{BA} + G_{CA}). \quad \text{(A8)}$$

The coefficient multiplying X on the right-hand side of Eqn. A8 is chosen to recover a properly normalized composition when the effect of the slab is neglected (or in the steady state). If we define L as a measure of the roughness amplitude,

$$L = \frac{1}{S} \int_{slab} d^3x\,\theta(\mathbf{r},t), \quad \text{(A9)}$$

we obtain from Eqn. A8, with the use of Eqn. A6,

$$\frac{d}{dt}\,\rho L X = SG_{BA} - SX\,(G_{BA} + G_{CA}). \quad \text{(A10)}$$

Assuming that L is a constant parameter and using the expression Eqn. A7 for ρ, we obtain the desired evolution equation for X:

$$\frac{dX}{dt} = \frac{1}{\alpha L}\,[X + \alpha(1 - X)]^2\,[V_{BA} - X\,(V_{BA} + V_{CA}/\alpha)]. \quad \text{(A11)}$$

Here, the precipitation fluxes $G_i = V_i/v_i$ (see Appendix 1) have been used, and $\alpha = v_{CA}/v_{BA}$ is the ratio of molar volumes.

APPENDIX 3

Growth Velocities

In this appendix, we obtain a relation of the form of Eqn. 12 and 13 for the species growth velocities. In the framework of the continuous growth mechanism, the growth velocity of $BaSO_4$ can be written as

$$V_{BA} = a_{BA} P_{BA}\,(\omega_+ - \omega_-), \quad \text{(A12)}$$

where a_{BA} is the size of a $BaSO_4$ molecule, ω_+ is the frequency of attachment of the molecule onto the surface of the crystal, ω_- is the frequency of detachment of the molecule from the surface, and P_{BA} is the probability of finding a kink site on the surface appropriate for $BaSO_4$ attachment. Generalizing the arguments of Markov (1996), the attachment is assumed to be an activated process, and its frequency is given by

$$\omega_+ = \nu m_A m_B v_{BA}^2 e^{-AU_{BA}/kT}, \quad \text{(A13)}$$

where ΔU_{BA} is the energy barrier for the incorporation of $BaSO_4$ into the crystal (related to the energy of desolvation) and $\nu \sim kT/h$ is a vibration frequency scale (h is Planck's constant, k is Boltzmann's constant, and T is temperature). The product $(m_A v_{BA})(m_B v_{BA})$ is basically the probability of finding the appropriate reactants in a region of volume v_{BA} in the vicinity of the attachment site. Similarly, the detachment frequency is given by

$$\omega_- = \nu[1 - \sum_{i=A,B,C} m_i v_{BA}]^2\, e^{-(\Delta U_{BA} + \Delta h_{BA})/kT}, \quad \text{(A14)}$$

where Δh_{BA} is the molecular enthalpy of precipitation. Again, the term in parentheses is basically the probability that the space around the detachment site is free of solute. At equilibrium, both frequencies are equal, so that

$$e^{-\Delta h_{BA}/kT} = \frac{(m_A m_B)^o\, v_{BA}^2}{[1 - \sum_{i=A,B,C} m_i^o v_{BA}]^2}, \quad \text{(A15)}$$

where $(m_A m_B)^o$ denotes the product of the equilibrium concentrations for which no net growth occurs, and m_i^o the corresponding equilibrium concentration. Finally, substituting Eqn. A13 to A15 in Eqn. A12 and neglecting the terms $m_i v_{BA}$ and $m_i^o v_{BA}$ compared to unity (which is valid for the dilute solutions which are of concern here), result in Eqn. 12 and 13. Similar relations are obtained for the growth of $SrSO_4$.